A new compartmental model - increased accuracy and precision of the traditional compartmental model without increased computational effort

K.A. Lindsay
Department of Mathematics, University of Glasgow,
Glasgow G12 8QQ

A.E. Lindsay
Department of Mathematics, University of Edinburgh,
Edinburgh EH9 3JZ

J.R. Rosenberg[†]
Division of Neuroscience and Biomedical Systems,
University of Glasgow, Glasgow G12 8QQ

July 16, 2004

[†] **Corresponding author**

J.R. Rosenberg
West Medical Building
Division of Neuroscience and Biomedical Systems
University of Glasgow
Glasgow G12 8QQ
Scotland UK

Tel (+44) 141 330 6589
Fax (+44) 141 330 2923
Email `j.rosenberg@bio.gla.ac.uk`

Keywords

Compartmental models, Dendrites, Cable Equation

Abstract

Compartmental models of dendrites are the most widely used tool for investigating their electrical behaviour. Traditional compartmental models assign a single potential to a compartment and consequently treat segments as isopotential regions of dendrite. All input is assigned to the centre of a segment independent of its location on the segment. By contrast, the compartmental model introduced in this article assigns a potential to each end of a segment, and takes into account the effect of input location on model solution by partitioning input between the axial currents at the proximal and distal boundaries of segments. For a given number of segments, the new and traditional compartmental models use the same number of locations at which the membrane potential is to be found. However, the solution achieved by the new compartmental model gives an order of magnitude better accuracy and precision than that achieved by a traditional model.

1 Introduction

Compartmental models have become important tools for investigating the behaviour of neurons to the extent that a number of packages exist to facilitate their implementation (*e.g.* Hines and Carnevale 1997; Bower and Beeman 1997). The use of compartmental models is motivated by the desire to reduce the mathematical complexity inherent in a continuum description of a neuron. This simplification is achieved by replacing the family of partial differential equations defining the continuum description of a neuron by a compartmental model of that neuron in which the behaviour of the neuron is described in terms of the solution of a family of ordinary differential equations (Rall, 1964). The traditional approach to compartmental modelling, introduced by Rall (1964), assumes that a "lump of membrane becomes a compartment; the rate constants governing exchange between compartments are proportional to the series conductance between them". Figure 1 illustrates the Rall interpretation of a how a dendrite can be represented in terms of compartments (neuronal membrane) and linking resistances (the axoplasm).

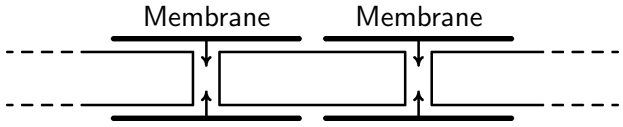

Figure 1: The Rall segmentation of a length of dendrite into lumped regions. The membrane defines the compartment, and the resistive property of the axoplasm is represented in the model by resistors linking compartments

This partitioning of a dendrite into repeating units is analogous to the representation of a transmission line as a ladder network of simple electrical circuits. In the case of a neuron, Rall defines a compartment to be the mathematical description of the effect of input acting on a localised region of neuronal membrane, and models this by an electrical circuit. The resistive properties of the axoplasm determine the linking resistances between compartments. Other authors (*e.g.* Segev and Burke, 1998) treat the neuronal segment, including the membrane and axoplasm, as the compartment. However both definitions lead to the same mathematical model simply because the iso-potential property, implicit in Rall (1964) and explicit in Segev and Burke's (1998) definition of a compartment, dominates the construction of the underlying family of ordinary differential equations. However, the definition of a compartment as an iso-potential region is unsatisfactory since a compartment defined in this way cannot act as a fundamental unit in the construction of a model dendrite for two good reasons. First, iso-potential compartments must exist in pairs to support axial current flow, and second, half compartments are required to represent branch points and dendritic terminals (*e.g.* Segev and Burke, 1998).

What is required is a definition of a compartment in which the compartment exists as an independent unit that can act as a building block for a model of the electrical behaviour of a neuron, where it is understood that "the function of the model is to represent the necessity that exists in nature by the logical necessity of the model. In the case of a good model one parallels the other"

(Regnier, 1964). A traditional compartmental model does not satisfy this criterion since its iso-potential structure provides no mechanism to differentiate between input *at different locations within the segment* represented by the compartment. It is precisely through the definition of a compartment, which allows this distinction to be made, that the new compartment model gives superior accuracy and precision to that of a traditional model.

The accuracy with which a compartmental model describes the behaviour of a neuron may be assessed from the knowledge that all compartmental models converge to the solution of the continuum model of that neuron as the maximum length of segment approaches zero. To take advantage of this result, a test neuron is constructed for which the continuum description has an exact solution. This test neuron and its exact solution are used as a reference against which the accuracy of a traditional compartmental model and the new compartmental model are compared.

2 Structure of compartmental models

We are concerned with compartmental models of dendrites. In this context, the fundamental morphological unit is the dendritic *section*, defined to be the length of dendrite connecting one branch point to a neighbouring branch point, to the soma or to a terminal. Compartmental modelling begins by subdividing each section of a dendrite into smaller contiguous units called segments which are typically regarded as uniform circular cylinders (*e.g.* Segev and Burke, 1998) or tapered circular cylinders (Hines and Carnevale 1997). The mathematical model of a dendrite is constructed by representing each segment by a compartment, and connecting these in a branching pattern corresponding to that of the dendrite. When joined in this way, each compartment interacts only with compartments representing adjacent segments. Note that some numerical schemes for the solution of the continuum model (*e.g.*, Finite Differences) may have this "nearest neighbour" property, but it would be a conceptual error to interpret such equations as a compartmental model. The "nearest neighbour" feature of these equations is a contingent property of the numerical algorithm[1] and vanishes with a different choice of algorithm, whereas the "nearest neighbour" feature of a compartmental model is unavoidable.

In a traditional compartmental model, the compartment has a single potential which is viewed as the potential at the centre of the segment represented by that compartment. This potential may be thought of as the average potential of that segment. All voltage-regulated input to the segment, independent of its location, acts with this potential. The assumption that all input to a segment acts with a single potential irrespective of location on the segment implies that a traditional compartmental model regards dendritic segments as iso-potential regions of dendrite.

[1]For example, a second order central difference approximation for the spatial derivatives of the continuum model will be structurally identical to a compartmental model when the error structure of the discretisation is ignored. However, the "nearest neighbour" property of the numerical algorithm is absent for a higher order finite difference scheme.

Spatial variations in biophysical properties of the dendrite and its morphology are expressed through differences in the properties of compartments and their linking resistors.

By contrast, the new compartmental model assigns two potentials to a compartment, one at each boundary of the segment represented by the compartment. Compartments constructed in this way can serve as the basic building blocks of a model dendrite because they sustain axial currents independent of neighbouring compartments. Most importantly, the assumption that transmembrane current acts at the centre of a segment, as in a traditional compartmental model, is now inappropriate and must be replaced in the new compartmental model by a rule to partition transmembrane current between the axial currents flowing at segment boundaries. As with the traditional compartmental model, compartments in the new model are connected together by enforcing conservation of axial current at segment boundaries, dendritic branch points and dendritic terminals.

3 Distributed and point input to a segment

In general, segments receive distributed and point sources of input each of which require a different mathematical treatment. The current supplied by distributed input such as intrinsic voltage-dependent current or capacitative current is proportional to the surface area of the segment on which it acts, whereas the current supplied to a segment at a synapse or by an exogenous point input is independent of the size of the segment. An implicit assumption of a compartmental model is that distributed current input to a segment is small by comparison with axial current flowing along the segment.

To appreciate why this assumption is reasonable, consider a cylindrical dendritic segment of radius r (cm), length h and with membrane of constant conductance g_{M} (mS/cm^2). Suppose that axoplasm has constant conductance g_{A} (mS/cm) and that a potential difference V (mV) exists between the segment boundaries, then the axial current along the segment is $I_{\mathrm{A}} = \pi r^2 g_{\mathrm{A}} V/h$ (μA) and the total distributed current crossing the membrane of the segment is $I_{\mathrm{M}} = 2\pi r h g_{\mathrm{M}}\,(V/2)$. The ratio of the distributed current to the axial current is therefore

$$\frac{\text{Distributed current}}{\text{Axial current}} = \frac{I_{\mathrm{M}}}{I_{\mathrm{A}}} = \frac{\pi r h g_{\mathrm{M}} V}{\pi r^2 g_{\mathrm{A}}\,(V/h)} = \frac{h^2 g_{\mathrm{M}}}{r g_{\mathrm{A}}} = \left(\frac{h}{r}\right)^2 \frac{r g_{\mathrm{M}}}{g_{\mathrm{A}}}\,. \tag{1}$$

For a typical dendritic segment $r g_{\mathrm{M}}/g_{\mathrm{A}}$ is small (say $\approx 10^{-5}$), and therefore distributed current acting on a segment is small by comparison with axial current for "short" segments. On the other hand, segments several orders of magnitude longer than their radius can be expected to have distributed and axial currents of similar magnitude. An important property of a compartmental model is that segments are not excessively long by comparison with their radius. In the treatment of distributed current, the development of the new compartmental model makes explicit use of the assumption that distributed current is much smaller than axial current. Since this assumption may not be valid for point sources of current, it will not be made for the treatment of these current in the new compartmental model.

3.1 Axial current in the absence of distributed and point current input

Figure 2 illustrates a dendritic segment of length h (cm) where $\lambda \in [0,1]$ is the fractional distance of a point of the segment from its proximal end ($\lambda = 0$). Let $r_{\rm P}$ and $r_{\rm D}$ be the radii of the segment at its proximal and distal boundaries respectively, let $V_{\rm P}(t)$ and $V_{\rm D}(t)$ be the membrane potentials at these boundaries and let $I_{\rm PD}$ be the axial current in the segment in the absence of transmembrane current.

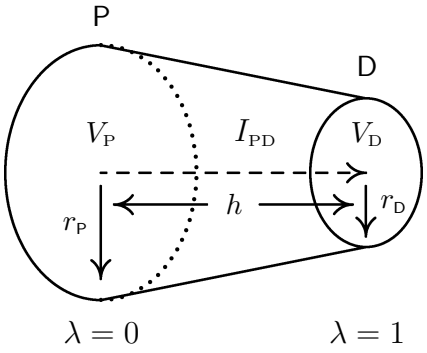

Figure 2: A segment of length h (cm) is illustrated. In the absence of transmembrane current, membrane potentials $V_{\rm P}$ and $V_{\rm D}$ at the proximal and distal boundaries of the segment generate axial current $I_{\rm PD}$.

The membrane of the segment in Figure 2 is formed by rotating the straight line PD about the axis of the dendrite to form the frustum of a cone of radius

$$r(\lambda) = (1-\lambda)r_{\rm P} + \lambda r_{\rm D}\,, \qquad \lambda \in [0,1]\,. \tag{2}$$

Assuming that the segment is filled with axoplasm of constant conductance $g_{\rm A}$ and that no current crosses its membrane, then the relationship between $V_{\rm P}$, $V_{\rm D}$ and $I_{\rm PD}$ can be constructed by integrating

$$I_{\rm PD} = -\frac{g_{\rm A}\pi}{h}\Big[\,(1-\lambda)r_{\rm P} + \lambda r_{\rm D}\,\Big]^2\,\frac{dV}{d\lambda}$$

with boundary conditions $V(0) = V_{\rm P}$ and $V(1) = V_{\rm D}$. This calculation shows that the potentials $V_{\rm P}$ and $V_{\rm D}$ give rise to axial current

$$I_{\rm PD} = \frac{\pi g_{\rm A} r_{\rm P} r_{\rm D}}{h}\,(\,V_{\rm P} - V_{\rm D}\,) \tag{3}$$

in the absence of distributed and point currents, and that the potential at point λ is

$$V(\lambda) = \frac{V_{\rm P}\,(1-\lambda)\,r_{\rm P} + V_{\rm D}\,\lambda\,r_{\rm D}}{(1-\lambda)\,r_{\rm P} + \lambda\,r_{\rm D}}\,. \tag{4}$$

Expressions (3) and (4) are estimates of the axial current flowing along a segment and the potential distribution within the segment in the absence of transmembrane current.

3.2 Motivation for partitioning point current input - model accuracy

One inescapable feature of a traditional compartmental model is that small variations in the location of segment boundaries, as might occur when a dendrite is represented by segments, may exert a large influence on the solution of the resulting mathematical model. Consider, for

example, a point input close to a segment boundary. A small variation in the position of that boundary may change the assigned location of this input from the centre of one segment to that of an adjacent segment. With respect to the mathematical model, the location of this input is therefore determined only to an accuracy of half a segment length, and this indeterminacy will in turn generate a model solution that is particularly sensitive to segment boundaries – small changes in these boundaries may lead to large changes in the model solution. Of course, with a small number of point sources of input, this problem can be avoided in a traditional compartmental model by arranging that only one point input falls on a segment, and that the location of this input coincides with the centre of the segment. However, this strategy is not feasible when dealing with large scale point input. What is required is a procedure that describes the effect of point input on a dendritic section in a way that is largely insensitive to how that section is represented by segments. It is essential to recognise that there are two primary sources of error in the construction of a compartmental model; the first is the well-documented effect of discretising a continuous dendrite, and the second pertains to error introduced by the placement of input on this dendrite. In a traditional compartmental model with n compartments, the first type of error is $O(1/n^2)$ (by analogy with the finite difference representation of derivatives), but it is not widely recognised that the second type of error is $O(1/n)$. Since the accuracy of any model must be governed by the least accurate contribution to the model, it is clear that *in practice* a traditional model is $O(1/n)$ accurate. This theoretical observation is supported by the simulation exercises of Subsections 7.1 and 7.2. By contrast with a traditional compartmental model, the new compartmental model describes the influence of input to an accuracy of $O(1/n^2)$, and therefore one would anticipate that it does not degrade the overall accuracy of the model. This assertion is testable by a simulation exercise.

3.3 Partitioning rule for transmembrane current

In compartmental modelling the effect of input current enters the mathematical model at points, or nodes, at which the membrane potential is known. In a traditional model, these nodes are at the centres of segments, whereas in the new model they are at the boundaries of segments. In the new model, input at any location is partitioned between the nodes at the proximal and distal boundaries of the segment on which the input acts. This procedure ensures that the solution of the mathematical model is insensitive to small changes in the location of segment boundaries simply because changes in these boundaries also affects how the input is partitioned between nodes.

In the mathematical model, the effect of input to a segment is treated as perturbations I_{P} and I_{D} to the axial current I_{PD} at the proximal and distal boundaries of a segment. Axial current $I_{\mathrm{PD}} + I_{\mathrm{P}}$ is assumed to leave the proximal boundary of a segment in the direction of its distal boundary, while axial current $I_{\mathrm{PD}} + I_{\mathrm{D}}$ is assumed to arrive at the distal boundary of a segment from the direction of its proximal boundary. The perturbations I_{P} and I_{D} must satisfy the

conservation of current condition

$$(I_{\rm PD} + I_{\rm D}) - (I_{\rm PD} + I_{\rm P}) + h\int_0^1 J(\lambda,t)\,d\lambda = 0 \quad \rightarrow \quad I_{\rm P} - I_{\rm D} = h\int_0^1 J(\lambda,t)\,d\lambda \tag{5}$$

where $hJ(\lambda,t)\,d\lambda + o(d\lambda)$ is the transmembrane current crossing the segment in $(\lambda, \lambda + d\lambda)$. The task is to construct expressions for $I_{\rm P}$ and $I_{\rm D}$ that satisfy (5) for all constitutive forms for $J(\lambda,t)$. In the new compartmental model, transmembrane current acting at point λ is divided between the proximal and distal boundaries of a segment in inverse proportion to the resistance of the segment lying between the point λ and that boundary. If $R_{\rm P}(\lambda)$ is the axial resistance of the portion of segment lying between the point λ and the proximal boundary of the segment, and $R_{\rm D}(\lambda)$ is the axial resistance of the portion of segment lying between the point λ and the distal boundary of the segment, then

$$R_{\rm P}(\lambda) = \frac{\lambda h}{\pi g_{\rm A} r_{\rm P} r(\lambda)}\,, \qquad R_{\rm D}(\lambda) = \frac{(1-\lambda)h}{\pi g_{\rm A} r_{\rm D} r(\lambda)}\,, \qquad R_{\rm P}(\lambda) + R_{\rm D}(\lambda) = \frac{h}{\pi g_{\rm A} r_{\rm P} r_{\rm D}}\,. \tag{6}$$

The rule for partitioning transmembrane current now leads to the expressions

$$I_{\rm P} = h\int_0^1 \frac{(1-\lambda)\,r_{\rm P}\,J(\lambda,t)\,d\lambda}{(1-\lambda)\,r_{\rm P} + \lambda\,r_{\rm D}}\,, \qquad -I_{\rm D} = h\int_0^1 \frac{\lambda\,r_{\rm D}\,J(\lambda,t)\,d\lambda}{(1-\lambda)\,r_{\rm P} + \lambda\,r_{\rm D}}\,, \tag{7}$$

which clearly satisfy identically condition (5) for the conservation of current.

3.4 Specification of transmembrane current

Transmembrane current is usually assumed to consist of four distinct components: capacitative current, intrinsic voltage-dependent current, synaptic current and exogenous current. Total transmembrane current is represented by

$$\int 2\pi r\,c_{\rm M}\,\frac{\partial V}{\partial t}\,dx + \int 2\pi r\,J_{\rm IVDC}(V)\,dx + \sum J_{\rm SYN}(V_{\rm syn}) + \sum I_{\rm EX} \tag{8}$$

where the integrals and summations are taken over the length of a segment. In this expression $c_{\rm M}$ (μF/cm^2) is the specific capacitance of the segment membrane, $V(x,t)$ is the distribution of membrane potential at time t (msec), $J_{\rm IVDC}(V)$ (μA/cm^2) is the density of transmembrane current due to intrinsic voltage-dependent channel activity, $J_{\rm SYN}(V_{\rm syn})$ (μA) describes synaptic input and $I_{\rm EX}$ (μA) describes exogenous input. Although the specific capacitance of dendritic membrane is normally taken to be constant in neuronal modelling, it will be treated here as a function of position to show how transmembrane current of this type may be incorporated into the new compartmental model. For a segment of length h, the expression for $J(\lambda,t)$ corresponding to formula (8) is

$$\begin{aligned} hJ(\lambda,t) \;\; = \;\; & 2\pi h r(\lambda)\,c_{\rm M}(\lambda)\,\frac{\partial V(\lambda,t)}{\partial t} + 2\pi h r(\lambda)\,J_{\rm IVDC}(V(\lambda,t)) \\ & + \sum_k J_{\rm SYN}(V_{\rm syn})\,\delta(\lambda-\lambda_k) + \sum_k I_{\rm EX}(t)\,\delta(\lambda-\lambda_k) \end{aligned} \tag{9}$$

where λ_k denotes the relative location of the k^{th} synapse or exogenous input with respect to the proximal boundary of the segment ($\lambda = 0$).

4 Representation of partitioned transmembrane current

Further progress requires expressions for $I_{\rm P}$ and $I_{\rm D}$ in terms of the biophysical and morphological properties of the segment and the membrane potentials at its proximal and distal boundaries. Each component of the transmembrane current (9) is examined separately.

4.1 Point sources of transmembrane current

There are two types of point sources of transmembrane current: point currents depending on transmembrane potential (synaptic current), often modelled by the constitutive equation $\mathcal{I} = g(t)(V - E)$ where E is the reversal potential associated with the synapse and $g(t)$ is the time course of the synaptic conductance, and those point currents which are independent of membrane potential (exogenous current).

Suppose that $\lambda_1, \cdots, \lambda_n$ are sites of point input $\mathcal{I}_1, \cdots \mathcal{I}_n$ to the segment, then the expressions for $I_{\rm P}$ and $I_{\rm D}$ are

$$I_{\rm P} = \sum_{k=1}^{n} \frac{r_{\rm P}}{r_k} (1 - \lambda_k) \mathcal{I}_k \,, \qquad -I_{\rm D} = \sum_{k=1}^{n} \frac{r_{\rm D}}{r_k} \lambda_k \mathcal{I}_k \tag{10}$$

where $r_k = (1 - \lambda_k) r_{\rm P} + \lambda_k r_{\rm D}$. In the special case of exogenous input only, $\mathcal{I}_k = \mathcal{I}_k(t)$ and expressions (10) give the exact partitioning of exogenous point input. When synaptic input is present, the expressions for $I_{\rm P}$ and $I_{\rm D}$ will contain the (unknown) membrane potentials at the synapses. The application of the partitioning rule will require these potentials to be estimated in terms of known functions and the potentials at the proximal and distal boundaries of the segment. One obvious way to do this is to use the potential distribution (4). However, the derivation of (4) assumed that transmembrane current was negligible by comparison with axial current, thus its efficacy in estimating the potential at a synapse relies on the validity of that assumption. It will be shown in Subsection 4.3.1 that the use of formula (4) for a single synapse overestimates the influence of that synapse. This observation suggests that the partitioning rule needs to be generalised to include situations in which point input current is not small by comparison with axial current.

4.2 Generalisation of partitioning rule for point input

The partitioning rule may be generalised by recognising that the partitioning of transmembrane current does not have to be between axial currents at the proximal and distal boundaries of the segment, but may be applied to nearest neighbour sites of a point input, although, of course, the proximal and distal boundaries of the segment may be nearest neighbours to one of these sites. This application of the partitioning rule is equivalent to considering the balance between axial current and point current at each input site ignoring the presence of distributed current between sites. Figure 3 is a schematic representation of a segment of length h illustrating the relative locations $\lambda_1, \cdots, \lambda_n$ of n point inputs $\mathcal{I}_1, \cdots \mathcal{I}_n$ on a segment. Suppose axial current

I_k flows to the point λ_k from the point λ_{k-1} and that V_k is the potential at the point λ_k.

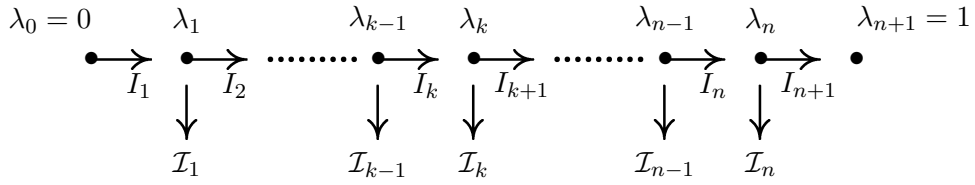

Figure 3: Configuration of point input to a dendritic segment of length h. Here $\mathcal{I}_k = g_k(t)(V_k - E_k)$ in the case of a synapse at λ_k or $\mathcal{I}_k = \mathcal{I}_k(t)$ in the case of an exogenous input.

The potentials $V_1, \cdots, V_n$ at the points $\lambda_1, \cdots, \lambda_n$ are related to the currents $I_1, \cdots, I_{n+1}$ by making the appropriate replacements in formula (3) to get

$$I_k = \frac{\pi g_{\text{A}} r_{k-1}\, r_k}{h(\lambda_k - \lambda_{k-1})} \left(V_{k-1} - V_k\right), \qquad k = 1, \cdots, (n+1) \tag{11}$$

where it is understood that $\lambda_0 = 0$, $\lambda_{n+1} = 1$, $r_0 = r_{\text{P}}$, $r_{n+1} = r_{\text{D}}$, $V_0 = V_{\text{P}}$ and $V_{n+1} = V_{\text{D}}$. It follows directly from (11) that

$$V_k = V_{\text{P}} - \frac{h}{\pi g_{\text{A}}} \sum_{j=1}^{k} \frac{(\lambda_j - \lambda_{j-1})}{r_{j-1}\, r_j}\, I_j\,, \qquad k = 1, \cdots, (n+1)\,. \tag{12}$$

If λ_k is the point of application of an exogenous input of strength $\mathcal{I}_k(t)$ then

$$I_{k+1} + \mathcal{I}_k(t) = I_k\,. \tag{13}$$

On the other hand, if there is a synapse at λ_k, then $\mathcal{I}_k = g_k(t)(V_k - E_k)$ and conservation of current requires that

$$I_{k+1} + g_k(V_k - E_k) = I_k\,. \tag{14}$$

Formula (12) for V_k is now used to rewrite equation (14) in terms of axial currents to get

$$I_k - I_{k+1} + \frac{g_k h}{\pi g_{\text{A}}} \sum_{j=1}^{k} \frac{(\lambda_j - \lambda_{j-1})}{r_{j-1}\, r_j}\, I_j = -g_k E_k + g_k V_{\text{P}}\,. \tag{15}$$

Thus, the current conservation condition at the points $\lambda_1, \cdots, \lambda_n$ gives rise to n equations for the $(n+1)$ currents $I_1, \cdots, I_{n+1}$. In order to complete the system of equations that determine $I_1, \cdots, I_{n+1}$, it is essential to note that the potentials at the proximal and distal boundaries of the segment are known, and that this condition constrains the values of these currents to satisfy

$$\frac{h}{\pi g_{\text{A}}} \sum_{j=1}^{n+1} \frac{(\lambda_j - \lambda_{j-1})}{r_{j-1}\, r_j}\, I_j = V_{\text{P}} - V_{\text{D}}\,. \tag{16}$$

This condition is obtained from equation (12) by asserting that $V_{n+1} = V_{\text{D}}$. Since it is the perturbations to the axial currents at the proximal and distal boundaries of the segment that are sought, and not the currents themselves, it is convenient to replace I_k in equations (13, 15

and 16) by $I_{\rm PD} + \widehat{I}_k$ where $\widehat{I}_k$ is the perturbation to I_k. If λ_k is the site of an exogenous input then it follows immediately that

$$\widehat{I}_k - \widehat{I}_{k+1} = \mathcal{I}_k(t)\,. \tag{17}$$

On the other hand, if λ_k is the site of a synapse, then the identity

$$\sum_{j=1}^{k} \frac{(\lambda_j - \lambda_{j-1})}{r_{j-1}\, r_j} = \frac{\lambda_k}{r_{\rm P}\, r_k}\,, \tag{18}$$

which can be established by induction, can be used to verify that $\widehat{I}_0, \widehat{I}_1, \cdots \widehat{I}_{n+1}$ satisfy

$$\widehat{I}_k - \widehat{I}_{k+1} + \frac{g_k h}{\pi g_{\rm A}} \sum_{j=1}^{k} \frac{(\lambda_j - \lambda_{j-1})}{r_{j-1}\, r_j}\, \widehat{I}_j = \mathcal{I}_k(t) \tag{19}$$

where the current $\mathcal{I}_k(t)$ is defined by the formula

$$\mathcal{I}_k(t) = g_k(t) \left[(1-\lambda_k) \frac{r_{\rm P}}{r_k}\, V_{\rm P} + \lambda_k \frac{r_{\rm D}}{r_k}\, V_{\rm D} - E_k \right]. \tag{20}$$

Note that $\mathcal{I}_k(t)$ is precisely the current that would be expected to flow at the k^{th} synapse if the distribution of potential along the length of the segment is well described by expression (4), that is, the potential distribution on the assumption that transmembrane current acting on the segment is negligible compared with axial current. Finally, equation (16) simplifies to

$$r_{\rm P}\, r_{\rm D} \sum_{j=1}^{n+1} \frac{(\lambda_j - \lambda_{j-1})}{r_{j-1}\, r_j}\, \widehat{I}_j = 0 \tag{21}$$

where the constant multiplier $r_{\rm P}\, r_{\rm D}$ has been added without loss to make the coefficients of this equation comparable to those appearing in the first n equations. Equations (17,19 and 21) may be represented compactly in matrix notation by

$$A\,\widehat{I} + GC\,\widehat{I} = \mathcal{I} \tag{22}$$

where $\widehat{I} = [\widehat{I}_1, \cdots, \widehat{I}_{n+1}]^{\rm T}$ is the $(n+1)$ dimensional column vector of perturbations in axial current, $\mathcal{I} = [\mathcal{I}_1, \cdots, \mathcal{I}_n, 0\,]^{\rm T}$ and A is the $(n+1) \times (n+1)$ matrix

$$\begin{bmatrix}
1 & -1 & 0 & \cdots & \cdots & 0 \\
0 & 1 & -1 & \cdots & \cdots & 0 \\
0 & 0 & 1 & \cdots & \cdots & 0 \\
\cdots & \cdots & \cdots & \cdots & \cdots & \cdots \\
0 & 0 & 0 & \cdots & 1 & -1 \\
\dfrac{\lambda_1 r_{\rm P} r_{\rm D}}{r_0 r_1} & \dfrac{(\lambda_2 - \lambda_1) r_{\rm P} r_{\rm D}}{r_1 r_2} & \dfrac{(\lambda_3 - \lambda_2) r_{\rm P} r_{\rm D}}{r_2 r_3} & \cdots & \dfrac{(\lambda_n - \lambda_{n-1}) r_{\rm P} r_{\rm D}}{r_{n-1} r_n} & \dfrac{(1 - \lambda_n) r_{\rm P} r_{\rm D}}{r_n r_{n+1}}
\end{bmatrix}. \tag{23}$$

Briefly, G is an $(n+1) \times (n+1)$ diagonal matrix in which the (k,k) entry is zero if λ_k is the site of an exogenous input and takes the value $g_k(t)$ if λ_k is the site of a synapse. The $(n+1, n+1)$ entry of G is always zero. The matrix C is a lower triangular matrix of type $(n+1) \times (n+1)$ in which all the appropriate entries in the k^{th} column take the value $(\lambda_k - \lambda_{k-1})/(\pi g_{\rm A} r_{k-1}\, r_k)$.

4.3 Special and general solutions of the point input partitioning equations

Prior to considering the general solution of equation (22) it is instructive to examine two special applications; the first concerns the derivation of the perturbations $I_{\rm P}$ and $I_{\rm D}$ in the case of a single synaptic input to a segment, and the second concerns the derivation of these perturbations in the presence of exogenous input only.

4.3.1 Single synaptic input

In the case of a single synaptic input at λ_1, equations (22) become

$$\Big(1+\frac{\lambda_1 h g_1}{\pi g_{\rm A} r_{\rm P} r_1}\Big)\widehat{I}_1-\widehat{I}_2=\mathcal{I}_1(t)\,,\qquad \frac{\lambda_1\widehat{I}_1}{r_{\rm P}r_1}+\frac{(1-\lambda_1)\widehat{I}_2}{r_1 r_{\rm D}}=0 \tag{24}$$

with solutions

$$I_{\rm P}=\widehat{I}_1=\frac{r_{\rm P}}{r_1}\,\frac{(1-\lambda_1)\mathcal{I}_1(t)}{1+\gamma}\,,\qquad -I_{\rm D}=-\widehat{I}_2=\frac{r_{\rm D}}{r_1}\,\frac{\lambda_1\mathcal{I}_1(t)}{1+\gamma}\,,\qquad \gamma=\frac{\lambda_1(1-\lambda_1)h g_1}{\pi g_{\rm A} r_1^2}\,. \tag{25}$$

Note that formulae (10) are recovered for a single synapse by setting $\gamma=0$ in the exact solutions (25). Therefore the use of formulae (10) overestimates the contributions made by the synapse at λ_1 to $I_{\rm P}$ and $I_{\rm D}$ whenever the potential at the synapse is estimated by expression (4). These overestimates are maximum when $\lambda_1=1/2$ – the synapse is located at the centre of the segment – and decrease with length of segment, and independently, with the state of synaptic activation.

In the case of a single synapse, the function γ describes the contribution made by the matrix GC in the determination of $I_{\rm P}$ and $I_{\rm D}$. The non-negative property of γ arises from the fact that the entries of G and C are always non-negative independently of the number of synapses. Consequently, if the influence of GC is ignored in the derivation of $I_{\rm P}$ and $I_{\rm D}$, the resulting values of these currents will overestimate the influence of the synaptic activity acting on the segment. Put another way, if transmembrane current due to synaptic activity is regarded as negligible by comparison with axial current, so that the potential distribution along the segment is determined from expression (4), then the resulting model will overestimate the influence of the synaptic activity.

4.3.2 Multiple point inputs

To take account of the influence of the matrix GC in the solution of equation (22), the algorithm

$$A\widehat{I}^{(m+1)}=\mathcal{I}-GC\widehat{I}^{(m)} \tag{26}$$

is iterated with initial condition $A\widehat{I}^{(0)}=\mathcal{I}$. Although it can be demonstrated that the matrix A has a simple closed form expression for its inverse, it is not (numerically) efficient to use this expression to solve equation (26). Instead, we observe that A has an LU factorisation in which U is the $(n+1)\times(n+1)$ upper triangular matrix with ones everywhere in the main

diagonal, negative ones everywhere in the super-diagonal and zero everywhere else, and L is the $(n+1)\times(n+1)$ lower triangular matrix

$$\begin{bmatrix} 1 & 0 & 0 & 0 & \cdots & \cdots & 0 \\ 0 & 1 & 0 & 0 & \cdots & \cdots & 0 \\ 0 & 0 & 1 & 0 & \cdots & \cdots & 0 \\ \cdots & \cdots & \cdots & \cdots & \cdots & \cdots & \cdots \\ \dfrac{\lambda_1\, r_{\rm P}}{r_1} & \dfrac{\lambda_2\, r_{\rm P}}{r_2} & \dfrac{\lambda_3\, r_{\rm P}}{r_3} & \dfrac{\lambda_4\, r_{\rm P}}{r_4} & \cdots & \dfrac{\lambda_n\, r_{\rm P}}{r_n} & 1 \end{bmatrix}. \tag{27}$$

Since $\mathcal{I}$ is a linear combination of $V_{\rm P}$, $V_{\rm D}$ and a voltage independent term, then the solution to equation (22) has general representation

$$\widehat{I} = \phi_1(t)V_{\rm P} + \phi_2(t)V_{\rm D} + \phi_3(t) \tag{28}$$

where $\phi_1(t)$, $\phi_2(t)$ and $\phi_3(t)$ satisfy

$$\begin{aligned} A\,\phi_1 &= \Big[\, g_1(1-\lambda_1)\frac{r_{\rm P}}{r_1},\ \cdots\ ,\ g_n(1-\lambda_n)\frac{r_{\rm P}}{r_n}, 0\,\Big]^{\rm T} - GC\,\phi_1\,, \\ A\,\phi_2 &= \Big[\, g_1\lambda_1\frac{r_{\rm D}}{r_1},\ \cdots\ ,\ g_n\lambda_n\frac{r_{\rm D}}{r_n}, 0\,\Big]^{\rm T} - GC\,\phi_2\,, \\ A\,\phi_3 &= -\Big[\, g_1E_1,\ \cdots\ ,\ g_nE_n, 0\,\Big]^{\rm T} - GC\,\phi_3\,. \end{aligned} \tag{29}$$

The equations (29) for $\phi_1(t)$, $\phi_2(t)$ and $\phi_3(t)$ may be solved easily by an iterative procedure based on the sparse LU factorisation of A. If the conductances $g_1,\ \cdots,\ g_n$ are sufficiently small, the solution of equations (29) is well approximated by ignoring the second term on their right hand side. This approximation is equivalent to using the partitioning rule (7) in combination with formula (4) for the membrane potential.

4.3.3 Exogenous input

If $\lambda_1,\ \cdots\ ,\lambda_n$ are sites of exogenous input $\mathcal{I}_1,\ \cdots \mathcal{I}_n$ then $G = 0$ in equation (22) and $\mathcal{I}$ is the vector of exogenous currents. In this case, expressions (10) for $I_{\rm P}$ and $I_{\rm D}$ are obtained immediately as the first and last entries in the solution $\widehat{I}$ of equation $A\,\widehat{I} = LU\,\widehat{I} = \mathcal{I}$.

4.4 Distributed transmembrane current

Distributed transmembrane current describes capacitative current and intrinsic voltage-dependent current, both of which are treated using equations (7) with appropriate expressions for $J(\lambda, t)$.

4.4.1 Capacitative transmembrane current

The component of capacitative current in (9) is estimated by approximating the true membrane potential along the segment by expression (4) based on zero transmembrane current to obtain

$$J^{\,\rm cap}(\lambda,t) = 2\pi c_{\rm M}(\lambda)r(\lambda)\frac{dV(\lambda,t)}{dt} = 2\pi c_{\rm M}(\lambda)\Big[\,(1-\lambda)\,r_{\rm P}\,\frac{dV_{\rm P}}{dt} + \lambda\,r_{\rm D}\frac{dV_{\rm D}}{dt}\,\Big]\,. \tag{30}$$

It now follows from expressions (7) that the contributions made by capacitative transmembrane current to I_{P} and to I_{D} are

$$\begin{aligned} I_{\mathrm{P}}^{\mathrm{cap}} &= 2\pi\, r_{\mathrm{P}} h\Big[r_{\mathrm{P}}\frac{dV_{\mathrm{P}}}{dt}\int_0^1 \frac{(1-\lambda)^2 c_{\mathrm{M}}(\lambda)\,d\lambda}{(1-\lambda)\,r_{\mathrm{P}}+\lambda\, r_{\mathrm{D}}} + r_{\mathrm{D}}\frac{dV_{\mathrm{D}}}{dt}\int_0^1 \frac{\lambda(1-\lambda)c_{\mathrm{M}}(\lambda)\,d\lambda}{(1-\lambda)\,r_{\mathrm{P}}+\lambda\, r_{\mathrm{D}}}\Big], \\ -I_{\mathrm{D}}^{\mathrm{cap}} &= 2\pi\, r_{\mathrm{D}} h\Big[r_{\mathrm{P}}\frac{dV_{\mathrm{P}}}{dt}\int_0^1 \frac{\lambda(1-\lambda)c_{\mathrm{M}}(\lambda)\,d\lambda}{(1-\lambda)\,r_{\mathrm{P}}+\lambda\, r_{\mathrm{D}}} + r_{\mathrm{D}}\frac{dV_{\mathrm{D}}}{dt}\int_0^1 \frac{\lambda^2 c_{\mathrm{M}}(\lambda)\,d\lambda}{(1-\lambda)\,r_{\mathrm{P}}+\lambda\, r_{\mathrm{D}}}\Big]. \end{aligned} \tag{31}$$

If the compartment is a uniform cylinder with constant specific membrane capacitance, the perturbations in axial current at the proximal and distal boundaries of the segment may be computed by evaluating the integrals in formulae (31) to get

$$I_{\mathrm{P}}^{\mathrm{cap}} = \frac{C}{6}\Big[\,2\frac{dV_{\mathrm{P}}}{dt}+\frac{dV_{\mathrm{D}}}{dt}\,\Big], \qquad -I_{\mathrm{D}}^{\mathrm{cap}} = \frac{C}{6}\Big[\,\frac{dV_{\mathrm{P}}}{dt}+2\frac{dV_{\mathrm{D}}}{dt}\,\Big] \tag{32}$$

where C is the total membrane capacitance of the segment. For tapered segments ($r_{\mathrm{P}} \neq r_{\mathrm{D}}$) with membranes of non-uniform specific capacitance, the integrals in (31) have values

$$\begin{aligned} I_{\mathrm{P}}^{\mathrm{cap}} &= 2\pi h\, r_{\mathrm{P}}\Big[c_{\mathrm{P}}\psi(r_{\mathrm{P}},r_{\mathrm{D}})+c_{\mathrm{D}}\phi(r_{\mathrm{P}},r_{\mathrm{D}})\Big]\frac{dV_{\mathrm{P}}}{dt} + 2\pi h\Big[c_{\mathrm{P}}r_{\mathrm{D}}\phi(r_{\mathrm{P}},r_{\mathrm{D}})+c_{\mathrm{D}}r_{\mathrm{P}}\phi(r_{\mathrm{D}},r_{\mathrm{P}})\Big]\frac{dV_{\mathrm{D}}}{dt}\,, \\ -I_{\mathrm{D}}^{\mathrm{cap}} &= 2\pi h\Big[c_{\mathrm{P}}r_{\mathrm{D}}\phi(r_{\mathrm{P}},r_{\mathrm{D}})+c_{\mathrm{D}}r_{\mathrm{P}}\phi(r_{\mathrm{D}},r_{\mathrm{P}})\Big]\frac{dV_{\mathrm{P}}}{dt} + 2\pi h r_{\mathrm{D}}\Big[c_{\mathrm{P}}\phi(r_{\mathrm{D}},r_{\mathrm{P}})+c_{\mathrm{D}}\psi(r_{\mathrm{D}},r_{\mathrm{P}})\Big]\frac{dV_{\mathrm{D}}}{dt} \end{aligned} \tag{33}$$

where $c_{\mathrm{M}}(\lambda) = (1-\lambda)c_{\mathrm{P}} + \lambda\, c_{\mathrm{D}}$ and the auxiliary functions $\phi(x,y)$ and $\psi(x,y)$ are defined by

$$\begin{aligned} \phi(x,y) &= \frac{x}{6(x-y)^3}\Big[x^2-5xy-2y^2+\frac{6xy^2}{x-y}\,\log\frac{x}{y}\,\Big], \\ \psi(x,y) &= \frac{x}{6(x-y)^3}\Big[2x^2-7xy+11y^2-\frac{6y^3}{x-y}\log\frac{x}{y}\,\Big]. \end{aligned} \tag{34}$$

The evaluation of the integrals in expression (31) is facilitated by defining the auxiliary integrals

$$\mathcal{K}_1 = \int_0^1 \frac{(1-\lambda)^2\widehat{c}_{\mathrm{M}}(\lambda)\,d\lambda}{\widehat{r}(\lambda)}\,, \qquad \mathcal{K}_2 = \int_0^1 \frac{\lambda(1-\lambda)\widehat{c}_{\mathrm{M}}(\lambda)\,d\lambda}{\widehat{r}(\lambda)}\,, \qquad \mathcal{K}_3 = \int_0^1 \frac{\lambda^2\widehat{c}_{\mathrm{M}}(\lambda)\,d\lambda}{\widehat{r}(\lambda)}$$

and observing that $\mathcal{K}_1$, $\mathcal{K}_2$ and $\mathcal{K}_3$ can be determined easily from the identities

$$\mathcal{K}_1+2\mathcal{K}_2+\mathcal{K}_3 = \int_0^1 \frac{\widehat{c}_{\mathrm{M}}(\lambda)\,d\lambda}{\widehat{r}(\lambda)}\,, \quad r_{\mathrm{P}}\mathcal{K}_1+r_{\mathrm{D}}\mathcal{K}_2 = \int_0^1 (1-\lambda)\widehat{c}_{\mathrm{M}}(\lambda)\,d\lambda\,, \quad r_{\mathrm{P}}\mathcal{K}_2+r_{\mathrm{D}}\mathcal{K}_3 = \int_0^1 \lambda\widehat{c}_{\mathrm{M}}(\lambda)\,d\lambda\,.$$

In particular, results for a uniform cylindrical segment ($r_{\mathrm{P}} = r_{\mathrm{D}}$) are obtained from formulae (33) by replacing $\phi(x,y)$ and $\psi(x,y)$ with their respective limiting values of $1/12$ and $1/4$ where each limit is taken as $x \to y$.

4.4.2 Intrinsic voltage-dependent transmembrane current

The construction of $I_{\mathrm{P}}^{\mathrm{cap}}$ and $I_{\mathrm{D}}^{\mathrm{cap}}$ for a membrane with non-constant specific capacitance provides the framework for treating intrinsic voltage-dependent transmembrane current. For an ionic species α, this current is usually described by the constitutive formula $J = g_\alpha(\boldsymbol{\theta})(V - E_\alpha)$ where V is the membrane potential, E_α is the reversal potential for species α and $g_\alpha(\boldsymbol{\theta})$ is

a membrane conductance which depends on a set of auxiliary variables $\boldsymbol{\theta}$, for example, the probabilities m, n and h appearing in the Hodgkin-Huxley (1952) model.

In the case of a *passive* membrane, the conductance $g_\alpha(\boldsymbol{\theta})$ takes a constant (but different) value for each species. The total transmembrane current density is obtained by summing the transmembrane current densities of each ionic species to get

$$J = \sum_\alpha g_\alpha(V - E_\alpha) = g_{\rm M}(V - E)\,, \qquad g_{\rm M} = \sum_\alpha g_\alpha\,, \quad E = \sum_\alpha \frac{g_\alpha}{g_{\rm M}}\, E_\alpha\,. \tag{35}$$

Thus the constitutive equation for the transmembrane current density of a passive membrane is $J = g_{\rm M}(V - E)$ where $g_{\rm M}$ (mS/cm^2) is the total membrane conductance and E plays the role of a reversal potential. When the segment is a uniform cylinder with a membrane of constant conductance, the contributions to $I_{\rm P}$ and $I_{\rm D}$ mimic formulae (32) for capacitative current and are respectively

$$I_{\rm P}^{\rm IVDC} = \frac{G}{6}\Big[\,2(V_{\rm P} - E) + (V_{\rm D} - E)\Big]\,, \qquad -I_{\rm D}^{\rm IVDC} = \frac{G}{6}\Big[\,(V_{\rm P} - E) + 2(V_{\rm D} - E)\Big] \tag{36}$$

where G is the total membrane conductance of the segment. Similarly, for tapered segments with non-constant membrane conductance, the contributions to the perturbations in the axial current at the proximal and distal boundaries of the segment are identical to expressions (33) with $c_{\rm P}$ replaced by $g_{\rm P}$ and $c_{\rm D}$ replaced by $g_{\rm D}$. These contributions are

$$\begin{aligned} I_{\rm P}^{\rm IVDC} &= 2\pi h\, r_{\rm P}\Big[g_{\rm P}\psi(r_{\rm P}, r_{\rm D}) + g_{\rm D}\phi(r_{\rm P}, r_{\rm D})\Big](V_{\rm P} - E) \\ &\qquad + 2\pi h\Big[g_{\rm P} r_{\rm D}\phi(r_{\rm P}, r_{\rm D}) + g_{\rm D} r_{\rm P}\phi(r_{\rm D}, r_{\rm P})\Big](V_{\rm D} - E)\,, \\ -I_{\rm D}^{\rm IVDC} &= 2\pi h\Big[g_{\rm P} r_{\rm D}\phi(r_{\rm P}, r_{\rm D}) + g_{\rm D} r_{\rm P}\phi(r_{\rm D}, r_{\rm P})\Big](V_{\rm P} - E) \\ &\qquad + 2\pi h\, r_{\rm D}\Big[g_{\rm P}\phi(r_{\rm D}, r_{\rm P}) + g_{\rm D}\psi(r_{\rm D}, r_{\rm P})\Big](V_{\rm D} - E) \end{aligned} \tag{37}$$

where the auxiliary functions $\phi(x, y)$ and $\psi(x, y)$ are defined in (34). At this stage of the development of the new compartmental model, all the expressions for the perturbations to the axial corresponding to each type of transmembrane current have been developed. It now remains to use these expressions to construct the model differential equations.

5 Construction of the model differential equations

Section 4 showed how the various components of point and distributed input can be partitioned between the proximal and distal boundaries of a segment. Once the total axial current $I_{\rm PD} + I_{\rm P}$ at the proximal boundary of a segment and $I_{\rm PD} + I_{\rm D}$ at the distal boundary of a segment are determined, the family of ordinary differential equations modelling the branched dendrite is constructed by enforcing conservation of current at all segment boundaries.

Each dendritic terminal at which the potential is unknown contributes one differential equation with form determined by the properties of the terminal. For example, if the terminal is sealed,

the differential equation expresses the condition $I_{\rm PD} + I_{\rm D} = 0$. At a dendritic branch point, the single differential equation is formed by equating the sum of the proximal current in the child segments to the distal current in the parent segment. A point soma behaves like a branch point with the current crossing the somal membrane playing the role of the distal current in the parent segment. Finally, at all other segment boundaries, the differential equation is constructed by equating the distal current of one segment to the proximal current of its neighbour.

Suppose that there are m nodes at which the potential is unknown, then the compartmental model of the neuron will be written for the potentials

$$V(t) = [\, V_1(t), V_2(t), \cdots, V_m(t) \,]^{\rm T} \,. \tag{38}$$

where $V_k(t)$ is the potential at the k^{th} node. The system of differential equations satisfied by $V(t)$ has general form

$$C\,\frac{dV}{dt} + G_{\rm SYN}(t)\,V + G_{\rm IVDC}(\boldsymbol{\theta}(t))\,V - AV + I(t) = 0 \tag{39}$$

where C, $G_{\rm SYN}(t)$, $G_{\rm IVDC}(\boldsymbol{\theta}(t))$ and A are $m \times m$ matrices such that their $(j,k)^{th}$ entry is non-zero whenever the j^{th} and k^{th} nodes lie at opposite ends of a segment, *i.e.*, they are neighbouring nodes. In equation (39), A is a constant matrix of axial conductances and C is a constant matrix of capacitances. The function $G_{\rm SYN}(t)$ is a matrix of time-dependent conductances associated with synaptic input to the dendrite, the function $G_{\rm IVDC}(\boldsymbol{\theta}(t))$ is a matrix of time-dependent conductances associated with intrinsic voltage-dependent transmembrane current to the dendrite, and $I(t)$ is a column vector of voltage-independent currents. Equation (39) is integrated over the interval $[t, t+h]$ to get

$$\begin{aligned} C[\,V(t+h) - V(t)] + \int_t^{t+h} G_{\rm SYN}(t)V(t)\,dt + \int_t^{t+h} G_{\rm IVDC}(\boldsymbol{\theta}(t))V(t)\,dt \\ - A\int_t^{t+h} V(t)\,dt + \int_t^{t+h} I(t)\,dt = 0\,. \end{aligned} \tag{40}$$

The trapezoidal rule is used to estimate each integral in equation (40) with the exception of the integral of intrinsic voltage-dependent current which is estimated by the midpoint rule. The result of this calculation is

$$\begin{aligned} C[V(t+h) - V(t)] + \frac{h}{2}\Big[G_{\rm SYN}(t+h)V(t+h) + G_{\rm SYN}(t)V(t)\Big] \\ + hG_{\rm IVDC}(\boldsymbol{\theta}(t+h/2))V(t+h/2) - \frac{h}{2}\Big[AV(t+h) + AV(t)\Big] \\ + \frac{h}{2}\Big[I(t+h) + I(t)\Big] + O(h^3) = 0\,. \end{aligned} \tag{41}$$

By noting that $2V(t+h/2) = V(t+h) + V(t) + O(h^2)$, equation (41) may be rearranged to give

$$\begin{aligned} \Big[2C - hA + h\,G_{\rm SYN}(t+h) + h\,G_{\rm IVDC}(\boldsymbol{\theta}(t+h/2))\Big]\,V(t+h) = \\ \Big[\,2C + h\,A - h\,G_{\rm SYN}(t) - h\,DG_{\rm IVDC}(\boldsymbol{\theta}(t+h/2))\,\Big]\,V(t) - h\Big[I(t+h) + I(t)\Big] + O(h^3). \end{aligned} \tag{42}$$

The computation of $G_{\mathrm{IVDC}}(\boldsymbol{\theta}(t+h/2))$ depends on how intrinsic voltage-dependent current is specified. For example, for a membrane following Hodgkin-Huxley kinetics, $G_{\mathrm{IVDC}}(\boldsymbol{\theta}(t+h/2))$ is specified in terms of the solutions of a set of auxiliary equations. In this case, it is well known that $G_{\mathrm{IVDC}}(\boldsymbol{\theta}(t+h/2))$ can be computed to adequate accuracy from $V(t)$ and the differential equations satisfied by the auxiliary variables (*e.g.*, see Lindsay *et al.*, 2001). The coefficient matrices in equation (42) are therefore determined by $V(t)$ and known prior to the determination of the potential $V(t+h)$.

5.1 Some additional comments

All compartmental models of a dendrite begin with a subdivision of its sections into contiguous segments. The segments, in turn, define the compartments of the mathematical model. Both the new and traditional compartmental models are based on the *same* morphological segments. In a traditional compartmental model, the distribution of membrane potential throughout a dendrite is described by the membrane potentials at the centres of dendritic segments. By contrast, in the new compartmental model the membrane potential throughout a dendrite is described by the potential at segment endpoints. The number of nodes at which potentials are to be determined, and consequently the numerical complexity of the problem, are identical in both types of compartmental model. Furthermore, both models involve nearest neighbour interactions, and so the structure of the differential equations describing either model is identical. Consequently benefits such as the existence of a sparse matrix factorisation of the matrix on the left hand side of equation (42) are enjoyed by both types of model.

Finally, it should be noted that the development of the new compartmental model highlights structural differences between the treatment of point input in this model and their treatment in a numerical procedure used to solve the partial differential equations of the continuum model. In the compartmental model, conservation of current is applied at each synapse to arrive at an equation connecting potentials at neighbouring nodes. In a numerical procedure (*e.g.*, finite elements or finite differences), the potential at synapses is estimated on the basis of the assumed representation of the potential between nodes. Consequently, numerical procedures often conserve current in an averaged sense, but not necessarily point-wise at a synapse. It is unclear to what extent such a treatment of synaptic input influences the accuracy of numerical schemes.

6 The model neuron

The comparison of the accuracy of the traditional and new compartmental models is based on the construction of a branched neuron for which the continuum model has a closed form expression for the membrane potential in response to exogenous input. This solution then stands as a reference against which the performance of the traditional and new compartmental models can be assessed. The most effective way to construct a branched model neuron with a closed

form solution for the membrane potential is to choose the radii and lengths of its sections such that the Rall conditions for an equivalent cylinder are satisfied (Rall, 1964). These conditions require that the sum of the three-halves power of the diameters of the child limbs is equal to the three-halves power of the diameter of the parent limb at any branch point, and that the total electrotonic length from a branch point to dendritic tip is independent of path. In particular, the electrotonic distance from soma-to-tip is independent of path. The model neuron used in our simulation exercises, illustrated in Figure 4, satisfies these conditions. When the Rall conditions are satisfied, the effect at the soma of any configuration of input on the branched model of the neuron is identical to the effect at the soma of the unbranched equivalent cylinder with biophysical properties and configuration of input determined uniquely from those of the original branched neuron (Lindsay *et al.*, 2003).

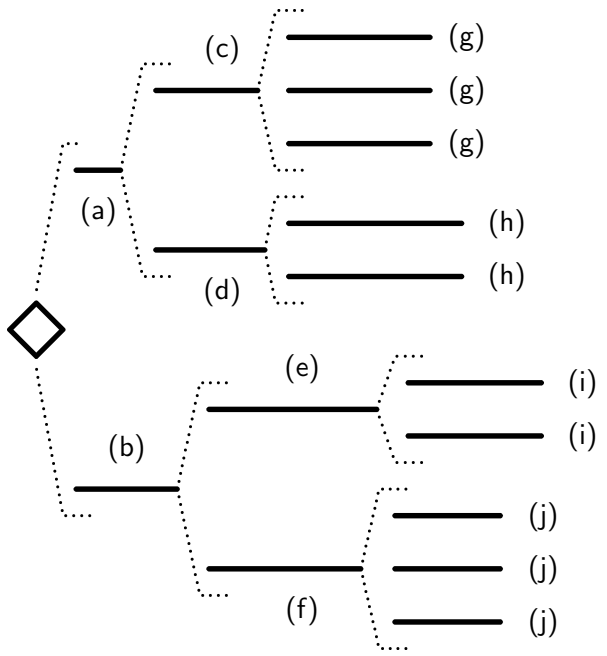

Section	Length μm	Diameter μm
(a)	166.809245	7.089751
(b)	379.828386	9.189790
(c)	383.337494	4.160168
(d)	410.137845	4.762203
(e)	631.448520	6.345604
(f)	571.445800	5.200210
(g)	531.582750	2.000000
(h)	651.053246	3.000000
(i)	501.181023	4.000000
(j)	396.218388	2.500000

Figure 4: A branched neuron satisfying the Rall conditions. The diameters and lengths of the dendritic sections are given in the right hand panel of the figure. At each branch point, the ratio of the length of a section to the square root of its radius is fixed for all children of the branch point.

To guarantee that any apparent errors between the closed form solution and the numerical solution from either compartmental model are not due to the lack of precision with which the branched dendrite is represented as an equivalent cylinder, a high degree of accuracy is used in the specification of dendritic radii and section lengths in the model neuron. The model neuron illustrated in Figure 4 is assigned a specific membrane conductance of $0.091\,\mathrm{mS/cm^2}$ (g_{M}) and specific membrane capacitance of $1.0\,\mu\mathrm{F/cm^2}$ (c_{M}), and axoplasm of conductance $14.286\,\mathrm{mS/cm}$ (g_{A}). With these biophysical properties, the equivalent cylinder has length one electrotonic

unit. The soma of the test dendrite is assumed to have membrane area $A_{\rm S}$, specific conductance $g_{\rm S} = g_{\rm M}$ and specific capacitance $c_{\rm S} = c_{\rm M}$.

6.1 Analytical solution

It may be shown that $V(t)$, the deviation of the somal transmembrane potential from its resting value as a result of a distribution $\mathcal{I}(x,t)$ of current on a uniform cylindrical dendrite of radius a and length l attached to a soma is

$$V(t) = e^{-t/\tau}\left[\,\phi_0(t) + \sum_\beta \phi_\beta(t) e^{-\beta^2 t/L^2\tau}\cos\beta\,\right], \qquad L = l\sqrt{\frac{2g_{\rm M}}{ag_{\rm A}}} \tag{43}$$

where τ is the time constant of the somal and dendritic membranes and $g_{\rm M}$ and $g_{\rm A}$ have their usual meanings. The summation is taken over all the solutions β of the transcendental equation $\tan\beta + \gamma\beta = 0$ where γ (constant) is the ratio of the total membrane area of the soma to the total membrane area of the dendrite. The functions $\phi_0(t)$ and $\phi_\beta(t)$ are solutions of the differential equations

$$\begin{aligned}
\frac{d\phi_0}{dt} &= -\frac{e^{t/\tau}}{C_{\rm D}+C_{\rm S}}\left[\,\mathcal{I}_{\rm S}(t) + \int_0^l \mathcal{I}(x,t)\,dx\,\right], \\
\frac{d\phi_\beta}{dt} &= -\frac{2e^{(1+\beta^2/L^2)t/\tau}}{C_{\rm D}+C_{\rm S}\cos^2\beta}\left[\,\int_0^1 \mathcal{I}(x,t)\cos\beta(1-x/l)\,dx + \cos\beta\,\mathcal{I}_{\rm S}(t)\,\right]
\end{aligned} \tag{44}$$

with initial conditions $\phi_0(0) = \phi_\beta(0) = 0$, that is, the neuron is initialised at its resting potential. The parameters $C_{\rm S}$ and $C_{\rm D}$ denote respectively the total membrane capacitances of the soma and dendrite, and $\mathcal{I}_{\rm S}(t)$ is the current supplied to the soma.

In the special case in which point currents $\mathcal{I}_1(t),\cdots,\mathcal{I}_n(t)$ act at distances $x_1,\cdots x_n$ from the soma of the uniform cylinder, the corresponding coefficient functions ϕ_0 and ϕ_β satisfy

$$\begin{aligned}
\frac{d\phi_0}{dt} &= -\frac{e^{t/\tau}}{C_{\rm D}+C_{\rm S}}\left[\,\mathcal{I}_{\rm S}(t) + \sum_{k=1}^{n} \mathcal{I}_k(t)\,\right], \\
\frac{d\phi_\beta}{dt} &= -\frac{2e^{(1+\beta^2/L^2)t/\tau}}{C_{\rm D}+C_{\rm S}\cos^2\beta}\left[\,\sum_{k=1}^{n} \mathcal{I}_k(t)\cos\beta(1-x_k/l) + \cos\beta\,\mathcal{I}_{\rm S}(t)\,\right].
\end{aligned} \tag{45}$$

7 Simulation exercises

Two different simulation exercises are used to compare the performance of the new compartmental model with that of a traditional compartmental model. The first simulation exercise assesses the performance of each type of compartmental model with respect to an analytical solution of the continuum model. In these simulations the NEURON simulator (Hines and Carnevale, 1997) is used to characterise the behaviour of a traditional compartmental model. The second simulation exercise compares the behaviour of a traditional compartmental model and the new compartmental model with respect to the spike train activity generated in each model by large

scale synaptic activity. In these simulations, a traditional compartmental model developed by the authors is used. The behaviour of this model in the first simulation exercise is indistinguishable from that of the NEURON simulator. Finally, all solutions of the compartmental models are advanced in one microsecond time steps to ensure that errors in temporal integration make no significant contribution to the error in the estimated membrane potential.

7.1 First simulation exercise

The performance of the traditional compartmental model is first compared against that of the new compartmental model by assessing the accuracy with which both models determine the time course of the somal potential of the model neuron (Figure 4) when subjected to large scale exogenous point input. The comparison relies on the fact that the model neuron has the property that the effect at its soma of an exogenous input at a given electrotonic distance from its soma is identical to the effect at the soma of that input acting on a uniform dendritic cylinder at the same electrotonic distance from the soma.

Each simulation distributes 75 point inputs at random over the dendritic tree of the model neuron, where each input has strength $2 \times 10^{-5}\,\mu$A. These inputs are then mapped to positions on the Rall equivalent cylinder at the same electrotonic distance from the soma (assumed to be a sphere of diameter $40\,\mu$m). The time course of the potential at the soma of the equivalent cylinder due to the combined effect of these inputs is determined analytically and taken to be the reference potential with respect to which error in both compartmental models is assessed. The potential at the soma in response to this stimulus regimen is obtained for the traditional and new compartmental models. The difference between a computed potential and its exact value is determined at one millisecond intervals in the first 10 milliseconds of the simulation, and each difference is divided by the exact potential at that time to get a relative measure of error at these times. The entire simulation procedure is now repeated 2000 times for each of 13 different levels of spatial discretisation (number of compartments).

7.1.1 Results

The results for the first simulation exercise of the traditional and new compartmental models are set out in Table 1. This table shows the common logarithms of the mean value of the modulus of the relative error and the standard deviation of that error estimated at ten milliseconds after the initiation of the stimulus and based on 2000 simulations for each level of spatial discretisation (number of compartments). Similar results, not shown, hold at all time points at which the errors were estimated.

Compartments ($\log_{10}$(Compartments))		NEURON	New Model	NEURON	New Model
		$\log_{10}$(Mean)		$\log_{10}$(Standard Dev.)	
17	(1.2305)	−2.41151	−2.71945	−2.62290	−3.19338
21	(1.3222)	−2.47233	−2.77674	−2.69851	−3.24583
34	(1.5314)	−2.94299	−3.41196	−3.06731	−3.88820
41	(1.6127)	−3.04729	−3.62138	−3.17081	−4.14997
54	(1.7323)	−3.21258	−3.89150	−3.34889	−4.41251
61	(1.7853)	−3.24692	−3.91268	−3.37653	−4.45051
75	(1.8750)	−3.35180	−4.12056	−3.46881	−4.65463
82	(1.9138)	−3.39846	−4.23567	−3.51591	−4.76498
93	(1.9684)	−3.45602	−4.30636	−3.57633	−4.82045
193	(2.2855)	−3.77417	−4.94731	−3.89829	−5.47886
293	(2.4668)	−3.94409	−5.31876	−4.07811	−5.84771
390	(2.5910)	−4.08234	−5.57349	−4.20025	−6.10791
495	(2.6946)	−4.15996	−5.78252	−4.28525	−6.32790

Table 1: The results of 2000 simulations for each of 13 different compartmental models based on the new and traditional (NEURON) representations of a compartment. The common logarithms of the mean value of the modulus of the relative error and the standard deviation of that error are estimated at ten milliseconds after the initiation of the stimulus.

The left hand panel of Figure 5 shows regression lines of the common logarithms of the modulus of the mean relative error for the traditional (dashed line) and new (solid line) compartmental models on the logarithm of the number of compartments used to represent the model neuron. These lines are based on the data in Table 1 and have equations

$$\begin{aligned} \log_{10}(\text{Mean Relative Error: NEURON}) &= -1.09 - 1.17\log_{10}(\text{Compartments})\,, \\ \log_{10}(\text{Mean Relative Error: New Model}) &= -0.17 - 2.10\log_{10}(\text{Compartments}) \end{aligned} \tag{46}$$

in which the regressions are achieved with respective adjusted R^2 values of 97.4% and 99.5%. In view of their very high R^2 values, a number of conclusions can be drawn from these results. For a fixed number of compartments, the error in the new model is always less than that of the traditional model. The regression equations (47) support the argument and subsequent assertion made in Section 3.2 that the error in a traditional compartmental model is approximately $O(1/n)$, whereas that in the new compartmental model is approximately $O(1/n^2)$. In practice, this means that the accuracy achieved by a traditional compartmental model using 500/100 compartments is achieved in the new compartmental model by the use of approximately 100/40 compartments.

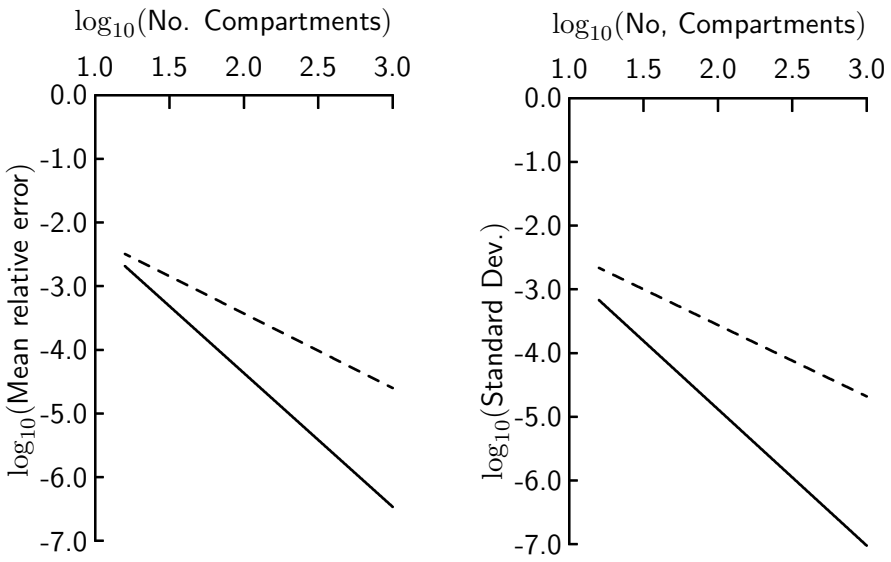

Figure 5: The left panel shows the regression lines of the mean relative errors in the new compartmental model (solid line) and that of a traditional compartmental model (NEURON - dashed line) against number of compartments. All errors are measured ten milliseconds after initiation of the stimulus. The right panel shows the regression lines for the standard deviations of the mean relative errors for the new compartmental model (solid line) and for a traditional compartmental model (NEURON - dashed line).

The standard deviation (SD) of the modulus of the relative error can be regarded as an indicator of the reliability of a single application of the model. The right hand panel of Figure 5 shows regression lines of the common logarithms of the standard deviation of the modulus of the relative error for the traditional (dashed line) and new (solid line) compartmental models on the logarithm of the number of compartments used to represent the model neuron. These lines are based on the data in Table 1 and have equations

$$\begin{aligned} \log_{10}(\text{SD of Relative Error: NEURON}) &= -1.32 - 1.12\log_{10}(\text{Compartments})\,, \\ \log_{10}(\text{SD of Relative Error: New Model}) &= -0.60 - 2.14\log_{10}(\text{Compartments}) \end{aligned} \tag{47}$$

in which the regressions are achieved with respective adjusted R^2 values of 98.7% and 99.4%. These lines show that the new compartmental model is more reliable than a traditional compartmental model. For example, a traditional compartmental model requires at least 100 compartments to give a standard deviation of the modulus of the relative error that is smaller than that of the new compartmental model using 40 compartments.

7.2 Second simulation exercise

In the second simulation exercise 100 synapses are distributed at random over the dendritic tree of the model neuron illustrated in Figure 4. Each synapse is activated independently of all other synapses, has a maximum conductance of 3×10^{-5} mS and a time constant of 0.5 msec.

Activation times for each synapse follow Poisson statistics with a mean rate of 30 pre-synaptic spikes per second. By contrast with the first simulation exercise in which the somal membrane was passive, the behaviour of the somal membrane in the second simulation exercise is active and obeys Hodgkin-Huxley kinetics. This simulation exercise is based on 12 different levels of spatial discretisation (number of compartments) in which each simulation of the traditional and new compartmental models use identical synaptic firing times and identical numbers of compartments.

7.2.1 Results

Table 6 gives the spike rate of soma-generated action potentials based on 11 seconds of activity, the first second of which is ignored.

Compartments ($\log_{10}$(Compartments))	Traditional Model Mean Firing Rate	New Model Mean Firing Rate
34 (1.5314)	31.5	27.6
41 (1.6127)	30.3	27.9
54 (1.7323)	30.5	27.5
61 (1.7853)	29.8	27.2
75 (1.8750)	29.2	27.0
82 (1.9138)	28.5	27.0
93 (1.9684)	28.3	26.8
193 (2.2855)	26.5	26.5
293 (2.4668)	25.9	26.2
390 (2.5910)	26.2	26.2
495 (2.6946)	26.7	26.2
992 (2.9965)	26.0	26.1

Table 2: The results of the second simulation exercise for a traditional compartmental model and the new compartmental model in which 10 second records of spike train activity are obtained for both models for 12 different levels of spatial discretisation (number of compartments).

Figure 6 illustrates the data set out in Table 2 in which the spike rates for the traditional model (dashed line) and new model (solid line) are plotted against the common logarithm of the number of compartments used in each simulation. As the number of compartments used in each model is increased, the spike rates generated by both models approach a common limit. However, the spike rate of the traditional model oscillates about this limit whereas that for the new model approaches the limit in a monotonic fashion, and achieves the limiting value with fewer compartments. For example, the spike rate obtained using the traditional model with

100 compartments is achieved with only 40 compartments in the new model. The spike rate obtained using the traditional model with 500 compartments is achieved in the new model with only 100 compartments. These differences in the number of compartments required to achieve the same level of accuracy in both models are identical to those observed in the first simulation exercise.

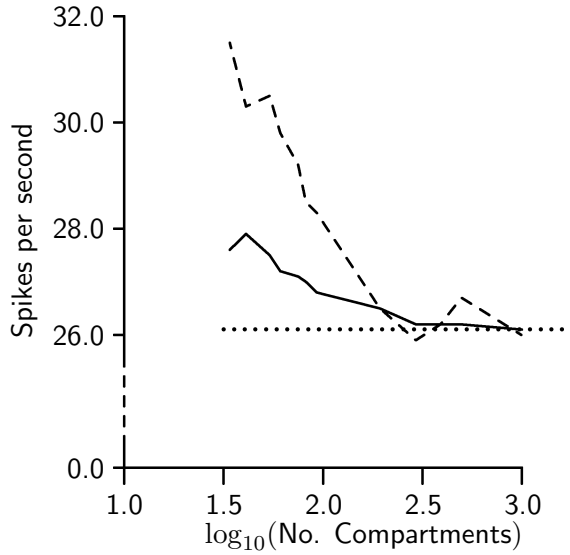

Figure 6: The spike rate plotted against the common logarithm of the number of compartments for a traditional compartmental model (dashed line) and the new compartmental model (solid line). The dotted line shows the expected spike rate.

8 Concluding remarks

This investigation has demonstrated that it is possible to achieve a significant increase in the accuracy and precision of compartmental models once the actual placement of input is reflected in the structure of the compartmental model. This finding is relevant to recent physiological studies that have demonstrated the extreme accuracy of the timing of events in spike trains (*e.g.*, Fellous *et al.*, 2001). To investigate this phenomenon it is essential that the numerical solution of the mathematical model accounting for this behaviour is sufficiently accurate to allow one to distinguish between different biophysical models. The simulation exercises demonstrate that the new compartmental model is better able to achieve this aim than a traditional compartmental model using an identical number of compartments.

Acknowledgement

A.E. Lindsay would like to thank the Wellcome Trust for the award of Vacation Scholarship (VS/03/GLA/8/SL/TH/FH).

References

Bower JM and Beeman D (1997) The book of GENESIS. 2nd ed. NY Telos.

Fellous J-M, Houlweling AR, Modi RH, Rao RPN, Tiesinga PHE and Segnowski TJ (2001) Frequency dependence of spike timing reliabilkity in cortical pyramidal cells and interneurons. *Journal of Neurophysiology* 85:1782-1787.

Hines M and Carnevale N (1997) The NEURON simulation environmment. *Neural Computation* 9:1179-1209.

Hodgkin AL and Huxley AF (1952) A quantatative description of membrane current and its application to conduction and excitation in nerve. *Journal of Physiology* 117:500-544.

Lindsay KA, Ogden JM, Halliday DM and Rosenberg JR (1999) An introduction to the principles of neuronal modelling. In *Modern Techniques in Neuroscience Research.* U Windhorst and H Johansson (eds.). Ch. 8, pp 213-306. Springer, Berlin.

Lindsay KA, Ogden JM and Rosenberg JR (2001) Dendritic sub-units determined by dendritic morphology. *Neural Computation* 13:2465-2476.

Lindsay KA, Ogden JM and Rosenberg JR (2001) Advanced numerical methods for modelling dendrites. In *Biophysical Neural Networks* RR Poznanski (ed.). Ch.15, pp 411-493. Mary Ann Liebert, Inc. New York.

Lindsay KA, Rosenberg JR and Tucker G (2003). Analytical and numerical construction of equivalent cables. *Mathematical Biosciences* 184:137-164.

Sonneveld P (1989) CGS, A fast Lanczos-type solver for nonsymmetric linear systems. *SIAM Journal of Scientific Statistical Computing* 10:36-52.

Rall W (1964) Theoretical significance of dendritic trees and motoneuron input-output relations. In *Neural Theory and Modelling.* R.F.Reiss (ed.). Stanford University Press, Stanford CA.

Regnier A (1966) *Les infortunes de la raison.* Les Éditions du Seuil. Paris.

Segev I and Burke RE (1998) Compartmental models of complex neurons. In *Methods in Neuronal Modeling - from ions to networks* 2nd Edition. Koch C and Segev I (eds.). Ch.3, pp 93-136. MIT Press, MA.